Quantum Information Processing, Vol. 4, No. 6, December 2005 (© 2006)
DOI: 10.1007/s11128-005-0007-9

Multiple RF Coil Nuclear Magnetic Resonance Quantum Computing

Lisa C. Siskind,[1] Bruce E. Hammer,[1,4] Nelson L. Christensen,[2] and Jeffrey Yepez[3]

Received July 7, 2005; accepted December 5, 2005; published online February 24, 2006

Recent work has demonstrated the feasibility of using an array of quantum information processors connected via classical channels (type II quantum computer) to implement a quantum lattice-gas algorithm. This paper describes work towards constructing a new experimental set-up for a type II quantum computer. This set-up has new hardware and software specifications but does follow previously published approaches of operation encoding the initial mass density onto a twoqubit processor and using standard pulse techniques to step through the algorithm. New hardware for this system includes the ability to read both qubits at once, effectively reducing the processing time by twofold. Hardware changes also include the use of multiple coils controlled by a single spectrometer and a hardware switch. New software includes a top level control system for the spectrometer for quick experimental configuration as well as configurable modeling software to verify results. Results are presented here from a system with the final software implementations and the two channel spectrometer configuration run on a single prototype coil. Progress towards the final multi-coil implementation is described.

KEY WORDS: Quantum information processing; nuclear magnetic resonance; quantum lattice gas; diffusion equation; quantum computing.

PACS: 03.67.Lx; 82.56.-b.

1. INTRODUCTION

Researchers in the newly emerging field of quantum information processing have made great strides both in its theoretical development and experimental practice during the last several years but progress is still strongly

[1] Center for Interdisciplinary Applications in Magnetic Resonance, University of Minnesota, Minneapolis, MN 55455, USA.
[2] Carleton College, Northfield, MN 55057, USA.
[3] Air Force Research Laboratory, Hanscom Field, MA 01731, USA.
[4] To whom correspondence should be addressed. E-mail: hammer@umn.edu

limited by the technological difficulty of accurately preparing and controlling the quantum state of many qubits. One successful approach to expanding the computational capabilities of current quantum information processing hardware is the construction of type II quantum computers. Type II quantum computers, as described in Refs. 1,2, constitute an ordered set of quantum processing nodes where inter-nodal information transfers is reducible to invertible quantum mechanical operators represented by orthogonal matrices – effectively inter-nodal communication via classical channels. This architectural paradigm allows for the use of several, uncorrelated quantum processors to speed computational times as a whole by working on separate parts of the problem: quantum parallelism occurs locally within a quantum node while classical parallelism occurs globally. A group from the Massachusetts Institute of Technology (MIT) has implemented one such device using a liquid state nuclear magnetic resonance (NMR) imaging technique and have achieved proof-of-concept by simulating the spacetime dynamics of a quantum lattice gas in 1+1 dimensions, modeling the macroscopic scale behavior of a many-body quantum system whose effective field theory is either the classical diffusion equation[3–5] or the classical nonlinear Burgers equation.[6,7] This type II system used a standard NMR setup with field gradients to spread out the magnetization signal from a single sample, containing two spin-1/2 nuclei, into 16 effective quantum computational nodes. While offering great advantages in increasing the number of computational nodes available, it also had the disadvantage of the complexity of the operations needed to encode and readout out data while still preserving the distinctness of the quantum nodes.[5]

This report describes our work towards implementing a different design for a type II NMR quantum computer intended to address the issues mentioned above.[6] Furthermore, this report presents new experimental results

[5]A newer version of the MIT approach attempts to employ a *k*-space encoding that directly implements the inter-nodal communication (or stream operator) using pulsed field gradients. This eliminates the need for continual readout of data after each time step.

[6]At University of Minnesota Center for Magnetic Resonance Research, a modern commercially available magnetic resonance imager called SENSE is used, arrays of four or eight different coils and receivers have been commonplace for the last five years. In some ways, they are built with vastly more sophistication than the idealized prototype system we have considered. Clinical SENSE coil arrays are a series of overlapping surface coils used to limit penetration and increase the signal to noise for imaging purposes. They are inappropriate for QIP applications for the following reasons. First, NMR QIP uses different nuclear spins to serve as qubits. This requires the use of multiple tuned or multiple coil NMR probe. Multi-frequency SENSE arrays are not presently available and will take a considerable engineering effort to develop. Second, QIP requires a highly uniform B_1 field for QIP calculations. SENSE coils have an inhomogeneous B_1 field due to their planar structure. Adiabatic pulses are not appropriate for NMR QIP because it takes milliseconds to achieve

as well as new NMR simulator results (modeling the operation and error sources in the NMR spectrometer) of the same quantum lattice-gas algorithm tested in Ref. 5. The main goals of this work are to explore this new hardware approach, improving efficiencies where possible, and streamlining and improving related data acquisition and control software as well as the simulator software. This work is the first step in an effort to construct a practical multi-coil system that can be quickly reconfigured and reused for testing different quantum computing algorithms.

Two key differences exist between our hardware design and the MIT design. The first is the simultaneous use of two receive channels as well as two output channels. This is in contrast to most system configurations that allow one or more send channels but are restricted to a single receive channel. This system can be scaled for additional send and receive channels as well. The advantage of simultaneous data readouts for each coil is twofold: the first is in performance and the second in accuracy. The system performance speed is doubled since the data can be obtained from two channels at once rather than having to read one channel, repeat the experiment, transfer the data from one channel to another and then read out the second channel. Furthermore, the experimental accuracy also improves since the data from both channels are obtained from the same run and not a repeat of the previous run; hence we can avoid errors from irreproducibility problems.

The second difference is using a one-to-one mapping of NMR coils to quantum computers as depicted in Fig. 1. This means as many coils are needed as desired quantum processors. This offers the advantage of relatively simple encode and read operations to operate each processor. It also allows the system to let nuclear spins contained within individual coils relax in preparation for the next computation while another coil is

---

a spin rotation versus microseconds in a conventional high homogeneity RF coil. Third, SENSE coils require precise geometric layouts. Crosstalk between small dimension SENSE coil arrays will pose significant, if not insurmountable, engineering challenges. They isolate themselves from one another by careful geometric arrangement of the coil layout. As the dimension of the coil decreases, the relative error in layout increases – thus making orthogonality of RF fields from adjacent coils more difficult. In contrast, in our approach the exact location of each microcoil, with respect to one another, is not critical. This is because the design goal is to have each microcoil be self-shielded, hence mitigating inter-nodal interaction. Positional uncertainty is not an issue in our case as it is with SENSE coils. Forth, typical SENSE coils have 20 dB isolation between channels. Under extraordinary conditions SENSE coils can have up to 60 dB isolation from one another. Crosstalk between channels will lead to decoherence in QIP experiments. Using individually shielded RF coils can provide isolation exceeding 100 dB thus providing higher immunity from decoherence. Finally, QIP uses ^{1}H, ^{13}C and other spin-labeled compounds to serve as qubits. A minimum of two qubits (different spins) are necessary for liquid sample QIP applications. Expensive "designer" molecules are necessary for two qubit applications, e.g., $^{13}CHCl_3$. Samples for QIP applications are mass limited and cannot use available SENSE coils due to filling factor and SNR considerations.

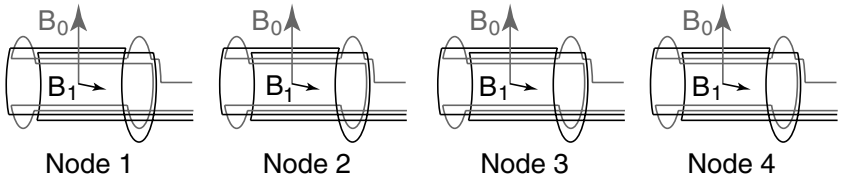

Fig. 1. Each coil acts as a quantum processor.

run by the central control processor and spectrometer, a type of pipelining. This is especially handy for samples with long T_1 times. Finally, this setup also allows for optimal use of costly spectrometer channels, increasing the system speed with the addition of more relatively inexpensive coils.

The MIT approach uses pulsed field gradients, decoupling and shaped radio frequency (RF) pulses to subdivide one sample into multiple quantum processors. It is difficult to create isolated quantum processing cells by this method. There is the potential for cross-talk between adjacent cells created by shaped RF pulses and gradients. The RF pulses are typically amplitude and phase modulated to create well defined spatial nodes. However, the dividing lines between the spatial nodes are not "brick walls" and thus the spins in adjacent slices are not completely isolated.

The use of shaped pulses also leads to a dispersion of phases within the selected slice. For many collision experiments there can be a significant accumulation of phase errors. The imaging approach also requires decoupling during the read portion of the experiment. This leads to partial spin polarization due to the nuclear overhauser effect (NOE).[8] NOE increase in signal strength for a carbon spin can be up to a threefold factor during proton irradiation and depends on the efficiency and duration of decoupling. This is an additional source of error when integrating the detected NMR signal.

A pulsed field gradient (PFG) is necessary to spatially map the spins. A PFG will induce eddy currents within the bore of an NMR magnet resulting in a time-dependent perturbation of the spins lasting long after the gradient is off. This can result in imperfect slices and unwanted frequency and phase shifts of the NMR spin ensemble. Note that PFGs are necessary for destroying off diagonal spin coherences during an NMR quantum information processing experiment and is a major source of error for both the imaging and multiple coil approach.

Finally, subdividing a sample by imaging methods results in a smaller signal to noise ratio (SNR) for the defined voxel than attainable by having a coil with a dimension equivalent to the voxel size. This observation is known as reciprocity and is the basis of matching the RF coil dimension to the sample size to optimize SNR.[9,10] The SNR for a specific nucleus at a fixed temperature is defined by

$$\frac{S}{N} \propto \frac{B_1}{I} \frac{V_s N \omega_o^2}{V_{noise}}, \tag{1}$$

where B_1/I is the RF coil sensitivity, V_s the sample volume, N the number of spins, ω_o is the larmor frequency and V_{noise} is the sample and RF coil noise voltage.[9,11] The term B_1/I represents a unit current induced in an RF coil from nuclear spins precessing in the transverse plane. This term becomes larger when spins coupling to the coil are physically close to the coil. So as the coil dimension decreases, nuclear spins are closer to the coil windings, thus inducing a larger current in the coil. The behavior of RF coils for mass-limited samples, i.e., a fixed number of spins, has been theoretically and experimentally investigated.[9,12] Generally, for a solenoidal RF coil the SNR per unit volume of sample is proportional to the inverse of the coil diameter for a coil diameter greater than 0.1 mm. For coils below 0.1 mm in diameter the per unit volume SNR is proportional to the square root of the coil diameter.

In addition to the new hardware features mentioned above, several custom software applications were created. The first was a highly reconfigurable control program that runs on the top layer of the experiment, controlling both the spectrometer software and coordinating the data collection and writing. This software was designed and written in a modular form and can be quickly reconfigured for different algorithms and experiments. The second software application was an NMR simulator to verify experimental results. This consisted of a Java user interface and a mathematica back-end. Again, both pieces were designed in a modular fashion for ease of reconfiguration and reuse.

For the initial work detailed in this paper, a single prototype hardware coil was used to simulate the behavior of 16 parallel coils. The software written for this NMR quantum computer experiment was designed for use with the multiple coil system.

This paper will first present a brief description of the quantum lattice gas system in Sec. 2. Section 3 describes the NMR implementation hardware and software. Section 4 shows the results of the first data run with the prototype coil and Section 5 provides a short summary and remarks about future work.

2. QUANTUM LATTICE GAS SYSTEM

The type II quantum algorithm can be exactly represented at the mesoscopic scale by an effective field theory: the *quantum Boltzmann equation* of motion that describes the time-dependent dynamics of a kinetic many-body particle system. The quantum algorithm is a novel computational

technique to reduce the complexity of fluid dynamics simulations where quantum logic operations directly causing qubit–qubit interaction are used to model the relevant local particle–particle interactions occurring within the fluid. The quantum model of the diffusion equation, in $D+1$ dimensions where D can be any number of spatial dimensions, requires only two qubits per node, and hence encodes the occupation of up to two particles at that node. An operator splitting method reduces the algorithmic complexity down to a modeling problem in $1+1$ dimensions.[13] This decomposition method in demonstrated for a $2+1$ dimensional test case in Ref. 14. The quantum algorithm then models unit-mass particle–particle interaction with one unitary collisional operation per lattice node per unit time step. In particular to model diffusion in $1+1$ dimensions, the $\sqrt{\text{SWAP}}$-quantum logic gate models the on-site particle–particle interaction. Once the interaction calculation is completed, the final algorithmic step of a single iteration of the time-dependent evolution of the quantum algorithm requires streaming the results (particle occupations) to the neighboring nodes. Both the collisional operation and the streaming operation conserve mass over the entire system. The orthogonal stream operator, $\mathscr{S}$, and its transpose (inverse), $\mathscr{S}^{\mathrm{T}}$, are the two informational transfer operations on the one-dimensional lattice, one operation per direction ($\pm x$). In the case where the particles have an equal probability of reversing direction in each interaction, the particle motion is effectively a random walk and the mass density field consequently diffuses isotropically over time.[5,15]

Our work concentrates on the implementation of the type II quantum algorithm in $1+1$ dimensions. This algorithm works by mapping the energy of each particle to the probability values of our quantum system and uses quantum state mixing to describe the interaction of particles.[5,16,17] Mapping the occupational probability onto the single-particle state of a quantum bit is done as follows:

$$|q\rangle = \sqrt{f}|1\rangle + \sqrt{(1-f)}|0\rangle. \tag{2}$$

A two qubit system is required for a one-dimensional quantum lattice representation of the diffusion equation. The initial wave function for such a system with f_1 and f_2 occupational probabilities is the following tensor product state:

$$\begin{aligned}|\psi(m,n)\rangle = {} & \sqrt{f_1(m,n)\,f_2(m,n)}|11\rangle + \sqrt{f_1(m,n)(1-f_2(m,n))}|10\rangle \\ & + \sqrt{(1-f_1(m,n))\,f_2(m,n)}|01\rangle \\ & + \sqrt{(1-f_1(m,n))(1-f_2(m,n))}|00\rangle,\end{aligned} \tag{3}$$

where m is the node index and n is the time-step index.

The four main steps of the type II quantum lattice gas algorithm are:

1. Encoding of the probability value for each qubit (i.e., f_1 and f_2).
2. Application of a unitary collision operator for quantum state mixing:

$$|\psi'(m,n)\rangle = \hat{U}|\psi(m,n)\rangle, \tag{4}$$

for all m where the $\sqrt{\text{SWAP}}$-quantum logic gate is

$$\hat{U} = \begin{pmatrix} 1 & 0 & 0 & 0 \\ 0 & \frac{1}{2}-\frac{i}{2} & \frac{1}{2}+\frac{i}{2} & 0 \\ 0 & \frac{1}{2}+\frac{i}{2} & \frac{1}{2}-\frac{i}{2} & 0 \\ 0 & 0 & 0 & 1 \end{pmatrix}. \tag{5}$$

3. Reading of the resultant probability values f_1' and f_2' (i.e., quantum state reduction).
4. Unitary streaming the results to the next site:

$$f_1(m,n+1) = f_1'(m-1,n), \tag{6}$$
$$f_2(m,n+1) = f_2'(m+1,n). \tag{7}$$

The reading method employed in this experiment follows the method of.[5]

3. NUCLEAR MAGNETIC RESONANCE IMPLEMENTATION

Liquid-state NMR was used for this implementation using a two gram sample of Carbon 13 labeled chloroform ($^{13}CHCl_3$) where the two spin-1/2 nuclei of hydrogen and the labeled carbon 13 comprised a two qubit system for ensemble quantum computing. A frequency difference, or *chemical shift*, of the spin-1/2 nuclei in the labeled chloroform is caused by the local magnetic fields within the molecule's geometrical structure. An external magnetic field B_0, on the order of a Tesla, creates a difference in population of the quantum states, between the aligned and anti-aligned spin-1/2 nuclei because of a small energy change in the Boltzmann weights at thermal equilibrium.[18] This energy difference is relatively small at room temperature but is still detectable due to the large number of molecules in the sample. Spin–spin coupling, mediated by correlated electrons within the molecule, further splits the ground state energy of one of the fermionic nuclei in the molecule depending on whether the other fermionic nuclei is spin up or spin down. This energy shift is much

smaller than the chemical shift, but is also clearly detectable. NMR spectrometers use high fidelity RF circuits to manipulate the net magnetization of the system and detect the population of each state as it returns to equilibrium. For the two qubit sample used above, the system is accurately described by the density matrix that depends on only the intramolecular spin degrees of freedom by tracing over all non-spin degrees of freedom, such as positional degrees of freedom, leaving a reduced 4×4 density matrix.

While NMR is technically advanced as compared to many quantum computing schemes due to the near 60-year history since the publication of the phenomenon of magnetic induction[19] there are still several technical challenges to the use of liquid-state NMR for quantum computing. Inhomogeneities in the background magnetic field and the RF coils cause spin–spin decoherence, limiting the number of quantum logic operational that can be executed with phase-coherence. Another problem is the relatively small number of controllable qubits within a molecule. Yet, the largest problem is the control of the pure quantum state of each molecule individually, which is not possible within the context of our experimental approach; hence the system is always in a mixed quantum state. Liquid-state NMR quantum computing was made possible with the development of several methods[20,21] for ensemble qubit preparation and the creation of start states that simulate pure quantum states. This work used the method described by Price *et al.*[22] for initial state preparation.

3.1. Mapping the Quantum Lattice Gas to the NMR Spin System

Much of this work, but not all, followed the same mapping scheme for the quantum state description to the physical experiment as in previous work.[5] One exception is the elimination of the need for the overall pulsed field gradient and a truncated RF modulation function for the discernment of different quantum processors. A summary of all the implementation differences are listed in Table 1.

3.2. Hardware

The basic elements of a NMR spectrometer setup are shown in Fig. 2. Components of the system include the magnet that provides the external magnetic field, the coil creating the orthogonal magnetic fields to manipulate the sample, the sample itself, a RF signal source that creates the pulse signals, a RF transmitter/receiver to prepare the outbound pulse and receive the resultant signal from the sample and finally the control computer for the whole system. In addition to the main components

Table 1. Implementation differences for type II quantum computer using imaging techniques versus separate coil design

Item	Pravia *et al* (5,16,17)	Multi-coil Implementation
Quantum Computer	Portion of a sample in a coil	One coil per quantum computer
Addressing	Via field gradient *possible crosstalk*, *possible eddy current artifacts*	By coil *no crosstalk*, *no eddy current artifacts*
Encoding	Shaped pulses *Decoupling needed*	Hard pulses *No Decoupling needed*
Reading	*Decoupling needed*	*No Decoupling needed*

needed, there are several key items for increasing the quality of the signal. Auxiliary magnetic shim coils are used within the magnet itself for increasing field homogeneity and for the creation of magnetic gradients. Pre-amps are used for increasing signal strength from the mixer and Transmit-Receive (TR) switches that allow the same coil windings to do dual duty as senders and receivers of signal from the sample.

A 1.5 Tesla large bore (55 cm) magnet was used for this experiment. The large bore allowed for the quick prototyping of a custom coil out of readily available materials. This bore can easily accommodate the addition of many more coils for the future expansion of this system. This is the planned next step in this work with the final goal being the construction of at least four coils working in parallel. The prototype coil used orthogonal Helmholtz-saddle circuits to independently control of each spin-1/2 ensemble via RF pulses.

The system described here differs from previous implementations of this algorithm[5,23] in that the entire RF coil is used as a single quantum computer. Previous implementations used a pulsed field gradient to split

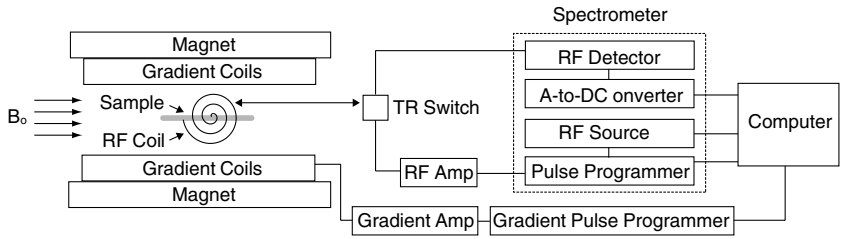

Fig. 2. Schematic overview of a NMR system.

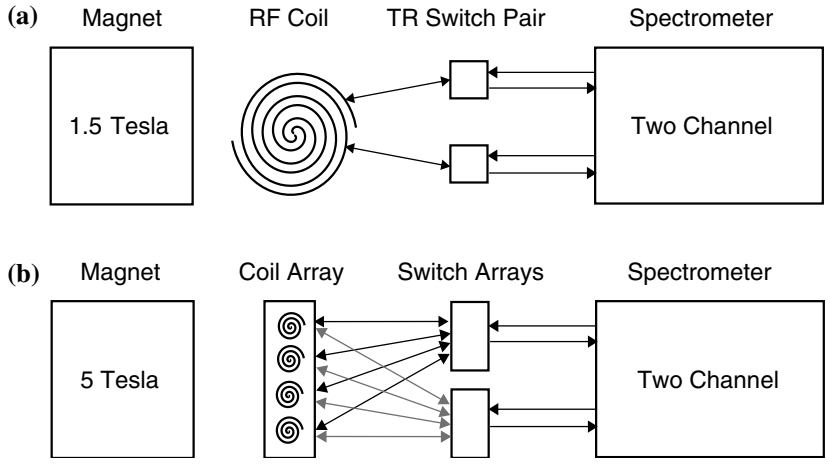

Fig. 3. (a) The prototype configuration shown above was used to obtain the data described in this work. (b) The new setup uses a four coil array, as shown in the final configuration schematic. The four coils are connected to a single multichannel spectrometer via a hardware switch. This switch allows the use of a single coil for a calculation while the remaining coils relax. This significantly improves the use factor for the spectrometer and magnet hardware since the relaxation time used between calculations for this work was 180 s, while the calculation sequence itself is executed in under a second. The use of four coils accessed round-robin instead of repeatedly using a single coil would allow a calculation to be executed every 45 s instead of once every 3 min, decreasing the overall experiment time needed by a factor of four.

a single coil into 16 effective quantum computational processors using NMR imaging techniques. While the single computer per coil design does force the construction of many coils versus the use of a single one, it also allows to us use hard pulses rather than shaped pulses for data encoding and to skip the use of decoupling sequences altogether for encoding and reading channels. It further eliminates artifacts from eddy currents induced by pulsed field gradients and possible crosstalk between adjacent cells due to imperfect slice selection from a truncated RF sinc function all through the use of independent coils.

The eventual goal of this work is to have several such coil quantum processors connected to the spectrometer via a hardware switch as shown in Fig. 3. This would allow the spectrometer to access one coil for a calculation while the remaining coils relax. This approach would significantly improves the use factor for the spectrometer and magnet hardware since the relaxation time used between calculations for this work was 180 s, while the calculation sequence itself is executed in under a second. The use of four coils accessed round-robin instead of repeatedly using a single coil would allow a calculation to be executed every 45 s instead of once every

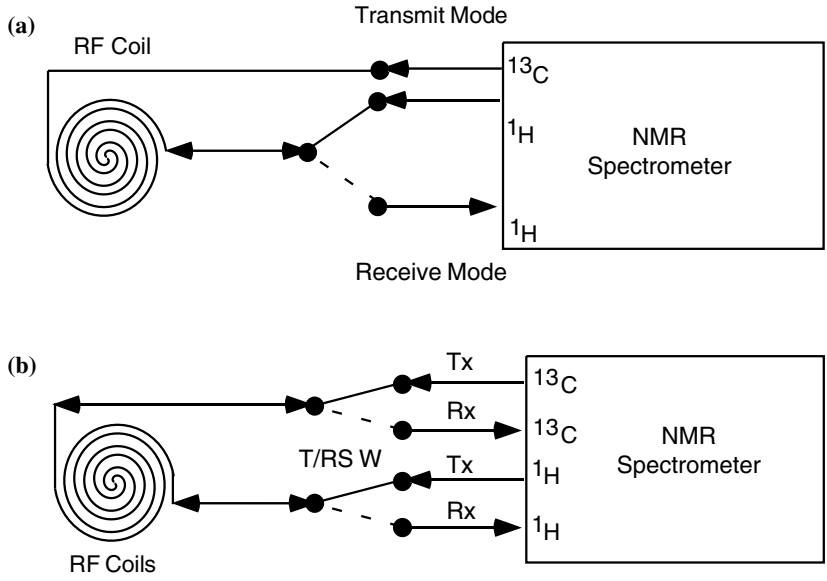

Fig. 4. (a) Classic spectrometer design with two send channels and a single receive channel. (b) Full two channel design configuration used for this work, containing two send as well as two receive channels.

3 min. This decreases the overall experiment time needed by a factor of four while still maintaining all the benefits of long decoherence times.

This approach is feasible within the physical parameters of existing NMR hardware. The magnet allocated for this final work is 210 mm useable bore 5.0 Tesla magnet with uniformity of 2 ppm for a 100 mm diameter spherical volume (DSV). Four individual 22 mm coils will be placed within in an array with center axis separation of roughly 45 mm, easily fitting within the 100 mm DSV. Shim and pulse power calibration parameters can be measured per coil and used by the software control program to minimize response differences between the coils. Additionally, the sample sizes used for these coils sizes are not much larger than those used for micro coils,[9,10] the use of which would allow even more coils to fit within the magnet's 100 mm DSV.

A custom built Apollo spectrometer (Tecmag, Inc., Houston, TX) was used to control the hardware system. This windows based unit was outfitted with two send as well as two receive cards which allowed for simultaneous control of both channels in all aspects of the experiment. This is shown schematically in the bottom section of Fig. 4. This system differs from the typical NMR spectrometer setup in that while many have multiple channels to send pulses out, few have more than one hardware channel

available for reading data. Thus most systems cannot look at the state of more than one qubit at the end of a computation. For a two qubit system this limitation would force an experimenter to run the same computation twice: once for the nominal qubit the channel was tuned to and a second time to read the data from the other qubit, using a swap operation to move the data over to the read-capable channel.

3.3. Control and Simulation Software Design

Custom software was written for both the control of the NMR quantum computer and the simulation software to verify the experimental results. Figures 5 and 6 show the designs for the experimental and the simulation software, respectively. A high level of encapsulation was used in the design for both systems. This allows for maximum reusability for the core code, meaning that core code written for this experiment could also be used for future experiments, whether a different algorithm for liquid state NMR quantum computing or even the same algorithm for solid state quantum computing.

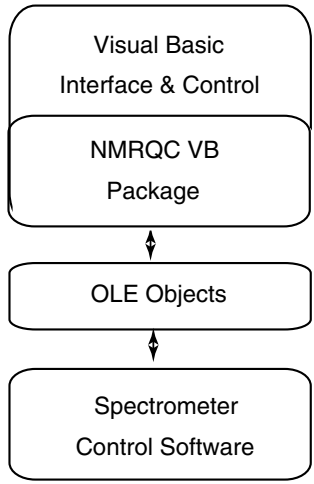

Fig. 5. High level architecture of the Experimental Control Software. This software is comprised of several layers: the top layer user interface and control module, the OLE objects used to communicate to the spectrometer and the spectrometer software itself. The top layer is designed to eventually be split into two separate layers as is denoted by the second object contained within it labeled "NMRQC VB Package". This package contains core NMR quantum computing commands needed for the execution of any quantum algorithm.

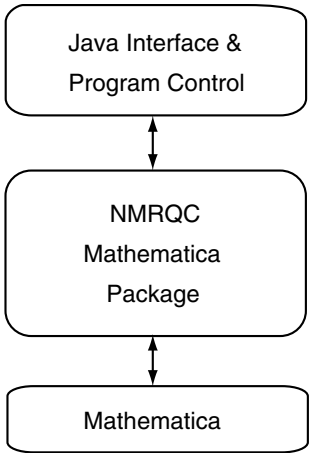

Fig. 6. Design of the Simulation Software. This software is comprised of several layers. The top layer contains the user interface and control module, all written in Java. The middle layer is the package of generic quantum computing Mathematica commands needed for the actual calculations. The middle layer also contains a few helper commands that combine many of the generic functions for quick communication. The bottom layer is the Mathematica engine itself that executed the commands and returns the results. Not explicitly shown is the J/Link communication package that facilitates communication between the Java application and the Mathematica software.

3.3.1. Experimental Control

The experiment was run using a Visual Basic software program developed to execute the algorithm logic and work as a higher layer of control over the spectrometer software. This allowed for precise timing between sequence executions as the sample reset to the thermal state. It also allowed for the automated analysis of results.

The Visual Basic program consisted of two layers: "User Interface and Control" and a core package of commands, "NMRQC VB Package", to access the Tecmag Objecting Linking and Embedding (OLE) objects[7] which were in turn used to control the spectrometer software and hardware.

The "User Interface and Control" layer accepted user input for experiment start values, provided a method to control the start of the experiment, coordinated the execution of all core commands needed to implement the algorithm and provided user feedback on the progress of an experiment underway. This allowed for the running of multiple

[7]OLE is a Microsoft developed standard for access and control of one program by another. The Tecmag software is written following the OLE standard and the company provides an Application Program Interface (API) guide for accessing these objects on their system.

experiments with different initial mass density distributions without the modification of a single piece of code.

The control layer also handled the saving and initial analysis of data. Data was stored as both raw spectrum files as well as final integrated values. The raw spectrum showed the state of the system over the duration of the experiment, as well as allowed the possibility of later applying multiple analysis methods, if so desired.

The layer just below the user interface, the "NMRQC VB Package", contained general commands needed for NMR quantum computing. This core code contained commands that are needed to run NMR quantum computing experiments in general, such as operations to initialize the system, encode values into each qubit and read out resulting values.

3.3.2. Pre-computed Experimental Overhead

In an ideal world, the sample response to RF power would be linear and could accurately be characterized by percent power needed per degree flip angle, which is in turn related to the spectral integral projection value by a sine function. This was not the case for the actual hardware in the real world. Others have found this to be true as well[16] and used a spy coil to record the actual response and adjust accordingly. The system used for this experiment was consistent enough to allow the use of a lookup table for actual found responses per RF power unit. The creation of this entailed the following steps:

1. The nominal RF power needed to flip the sample spectra 180 degrees in 180 or 240 μs was found, depending on the system used.
2. The RF power was divided into 28 equal parts.
3. The overall time used for the RF pulse was reduced by a factor of two so the nominal 180 power should produce a 90 degree pulse.
4. Spectra integral values were measured for the 28 RF pulse intervals chosen above plus another additional division in the event of undershooting the initial 180 degree power for a total of 29 RF power intervals.

These steps were repeated for each channel used. This created a lookup table of percent maximum response per percent input power. For the running of the actual experiment needed RF pulse powers were interpolated between lookup table values as needed. Figure 7 shows the data for the 1.5 Tesla system.

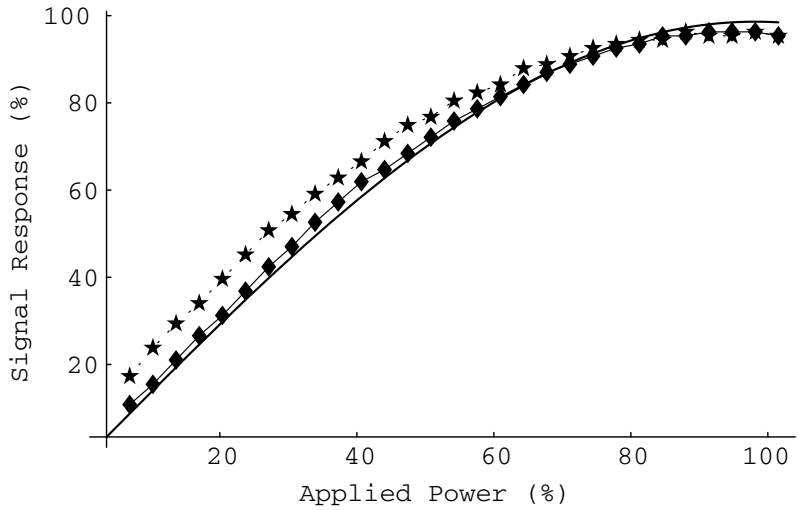

Fig. 7. The percent of maximum signal response, per percent input RF power from the spectrometer software. Twenty nine divisions were used to measure the overall system signal response. These are the maximum power divided by 28, plus another increment to verify that the maximum power was not under-estimated. The maximum power value was determined during an initial calibration process as the power needed to produce a 90 degree flip, i.e., the maximum signal. The diamonds are channel one and the stars are channel two. A sine curve, showing the theoretical power response, is fitted to channel one and is shown as the solid line.

3.3.3. Simulation of Expected Results

Experimental results were verified through a separate simulation program. This program also follows the multilayer paradigm, as shown in Fig. 6, for a high level of code reuse. This software consists of two main sections: a core Mathematica package containing all the quantum state manipulations necessary and a top-layer java application written to access the Mathematica engine through the Mathmatica toolkit J/Link. This design allows the top layer java application to evaluate different user input, load the core quantum computing package, execute the desired simulation and quickly return well formated results. The benefits of such a design are multi-fold: the top layer user interface allows different inputs to be evaluated nearly instantaneously without any re-coding, standardized graphical user interface tools can be used, along with standardized logging techniques for the results, and finally, the lower layer core Mathematica package can be reused for new quantum algorithm experiments.

The simulator program calculated two sets of data. The first is an ideal calculation dataset that assumes perfect encoded values and zero

error terms, for each cell of our simulated lattice. The second dataset evaluates the addition of user specified errors in the implementation, such as incorrect system calibration and outside noise. The error terms specification allowed for the evaluation of both systematic as well as random errors. The systematic errors analyzed included incorrect flip angle power calibration, which would introduce overall under or overshooting of the intended angle, incorrect initial value encoding error, which is also a flip operation but was analyzed separately, incorrect evolution timing, overall signal loss and incomplete gradient applications. Random errors analyzed included random flip angle errors, evolution errors and encoding errors.

Systematic errors were modeled by using a multiplier of magnitude selected by the user. It could be positive or negative. All operations using the selected operation were equally affected. Selecting an error of 0 is the same as executing the ideal calculation. Furthermore, random errors were also propagated by a multiplier but this time using a random number generator to selected a number within plus or minus the user selected value. A new random number was selected for each occurrence of the operation, and for each iteration.

Overall loss was calculated by reducing the final output matrix values by the user selected amount at the end of each complete calculation. This was performed once per calculation cell per iteration.

Incomplete gradient application was calculated by attenuating the density matrix off-axis values to a user selected percentage. Ideally, the application of a gradient reduces all off-axis terms of the density matrix to zero. The result of this application was the existence of off-axis terms after the application of a gradient. This error was termed gradient "leakage," since the magnitude denoted the percent of off-axis terms remaining.

3.4. Quantum Lattice Gas Simulation

Figure 8 shows the steps involved in one calculation cycle. The first portion manipulates the state density into the pseudo-pure start state.[22,24,25] This is a much simpler start state then the nominal room temperature mixed state, both equalizing the Hydrogen and Carbon signals and eliminating off-axis and mixed states. Once this is accomplished, the system is encoded with the desired start values. Both qubits are encoded at the same time followed by the application of the collision operator. Finally, the values of both qubits are read.

Using hard pulses and separate coils for each calculation rather than imaging techniques to divide the sample into effective cells in frequency space eliminates the need for decoupling during encoding and reading of data. A small spread in frequency space does not impact the accuracy of the separate coil implementation since it does not use that domain to define the

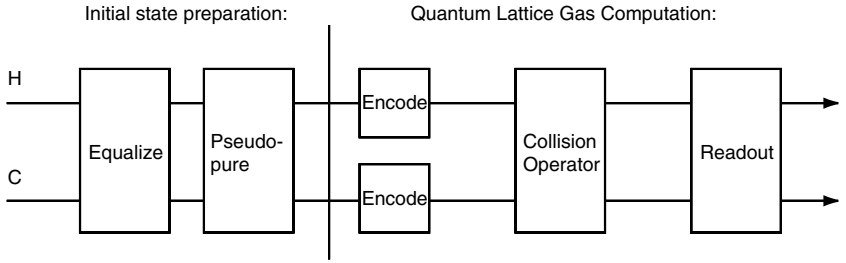

Fig. 8. The pulse sequence of single time step for the NMR implementation of the quantum lattice-gas algorithm. The first steps prepare the sample for a calculation by equalizing the spin signals and then setting them into a pseudo-pure state. Once this is done, each spin ensemble is encoded with the desired starting values. The collision operator is applied to the sample and final values of the resultant density values are ready out. Both channels are read at the same time. Hard pulses are used throughout.

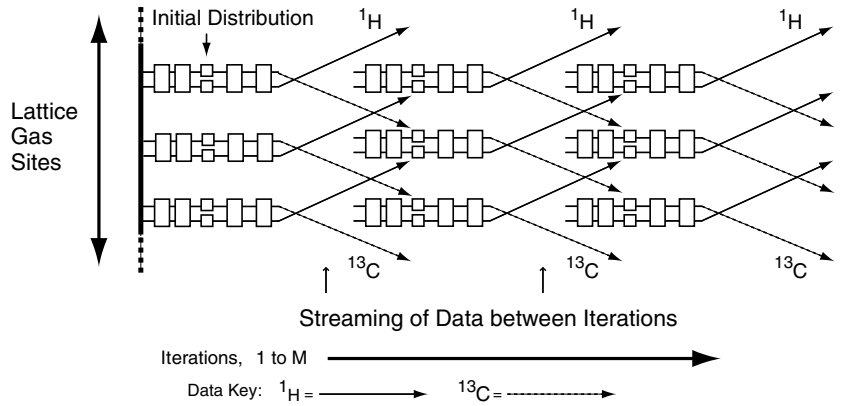

Fig. 9. The data flow for the lattice-gas algorithm, adapted from.[16] The calculations for the algorithm were run one at a time on the single prototype coil, simulating the action of 16 different coils running simultaneously for each iteration of the algorithm. See Fig. 8 for details on each quantum circuit. The read values for each calculation were streamed to the next encode step at the appropriate location in the lattice for the next iteration: the hydrogen moving up one step and the carbon moving down one step between each iteration.

calculation cells themselves. This saves in both execution time and accuracy. Both channels were encoding during a single 90 μs pulse time step rather than the two 8 ms pulse intervals needed to encode the data for the previous implementation using imaging techniques.[5] Additionally, exposure to well know decoupling error terms such as the NOE are eliminated.

Figure 9 shows the flow of data over the course of the entire experiment. Values are streamed between iterations. A continuous boundary

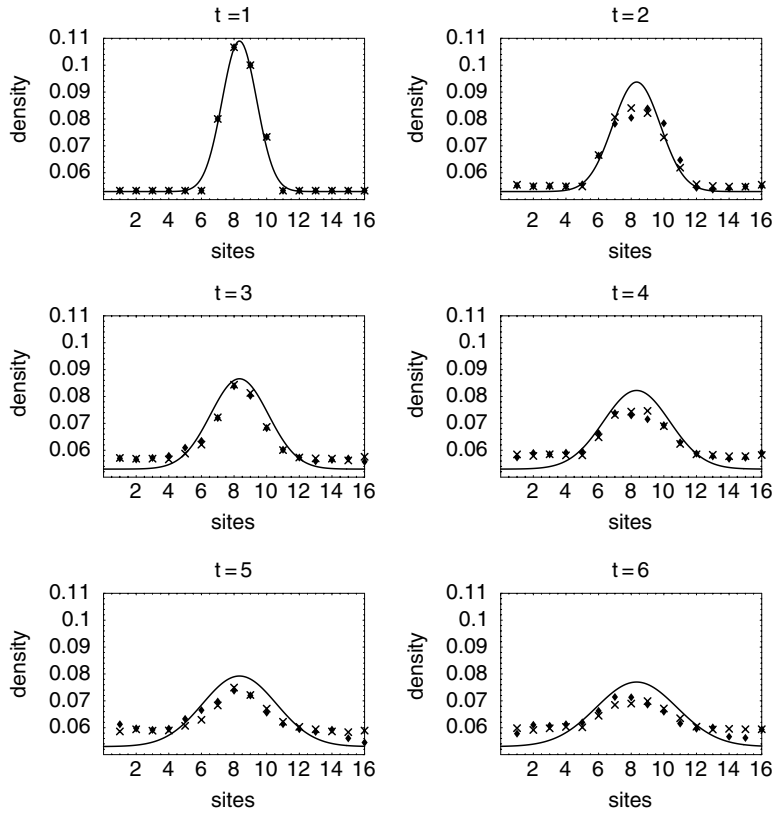

Fig. 10. Ideal (solid curve), experimental (diamonds) and simulated (crosses) values for the 16 cells of the quantum lattice-gas algorithm over six time steps. The algorithmic time labels each snapshot. For each graph, cells number one through 16 are shown along the bottom from left to right. The cell values of the total number density are shown vertically.

condition is met by having the values of quantum computation cell 16 streamed to cell 1 and vice versa.

4. EXPERIMENTAL RESULTS

Figure 10 shows the ideal, actual and simulated data for the 1.5 Tesla system. There is good over all agreement between the analytical solution and experimental values in terms of the overall shape, but there is an overall growth in the density values across all cells for each iteration of the algorithm.

The experimental data was simulated with reasonable agreement using the error values shown in Table 2. Analysis of the data presented

Table 2. Simulator error values used to model the experimental data

Item	Systematic (%)	Random (+/−%)
Error values used for simulated data		
Evolution	−2.0	0.5
Flip	3.5	0.5
Proton encode	−4.0	0.5
Carbon encode	−2.0	0.5
Overall loss	1.0	0.0
Gradient leakage	35	n/a

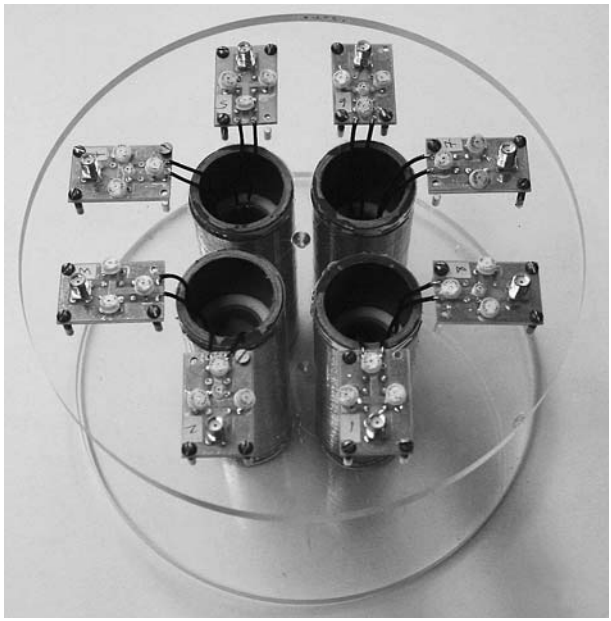

Fig. 11. A four coil array. Helmholtz coil pairs were implemented on 22 mm outer diameter G10 fiberglass tubing and mounted within 38 mm outer diameter RF copper shields. The copper shields which were constructed of electrically isolated strips of copper overlaid on fiberglass tube to form a complete physical barrier. The four coil and shield units were then mounted on two plexi-glass discs of 20.8 cm diameter that would slide within the 21 cm bore of the 5 Tesla magnet and maintain consistent coil placement from experiment to experiment. Holes within the plexi-glass discs allowed for sample placement within the coils and connections of the coils to the tuning boards. Each coil pair was tuned to 212.5 and 53.4 MHz, the Larmor resonant frequencies of H^1 and C^{13}, respectively.

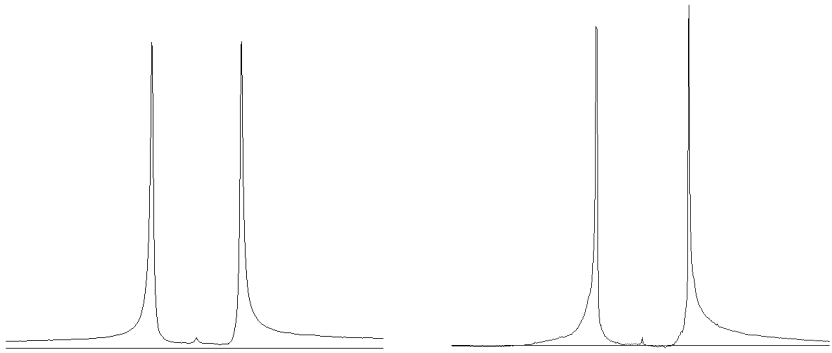

Fig. 12. ^{1}H spectra for the magnets and coil positions used for this work. The upper left shows the spectra in the 1.5 Tesla magnet with the coil centered. The upper right shows the results in the 5 Tesla magnet, again with the coil centered. Finally, the bottom image shows the results for one of the coils in coil array, where the coil itself is off-center from the magnet's central axis, nominally the region of maximum B_0 uniformity. The full-width, half maximum (FWHM) line widths for each of these is approximately 10, 5 and 7 Hz, respectively.

here showed that the incomplete elimination of off-axis elements for pseudo-pure start state appeared to be the dominant error term. This approach relies on gradients to eliminate these off-axis elements. However, eddy currents caused by gradients can interfere with the temporal field homogeneity, distorting the results of the calculation sequence beyond use. For this reason our pulse power of the existing gradient coil magnet insert was limited. The data presented here shows a compromise between gradient coil power and distortions caused by field inhomogeneities due to eddy currents. One approach to address this issue is to use individual gradient

coils around each processor coil for future hardware implementations. The increased distance between the gradient coils and the magnet walls would allow for much stronger gradient pulses without the penalties of eddy current induced field distortion and would have a significant impact on the results.

The incomplete elimination of the off-axis terms is also significant in that this had a multiplicative effect on other error terms. One example is finding that the resultant errors for flip angle inaccuracies are double the expected values when a high degree of off-axis terms remained. This amplification effect is also seen to a lesser degree for evolution errors. A key indicator that off-axis terms are present is the non-symmetric growth of error in each channel. This behavior is generally not seen with the other error terms studied, with the possible exception of random noise, which is at least a magnitude smaller in effect.

Overall signal loss, or decoherence plays a key role in the appearance of the data. Even small overall signal loss (one percent or less) from time of density encoding to final read resulted in the appearance of an asymptotic limit to the density values over several iterations. This signature shape was not seen from other error terms studied.

Finally, the system was equally sensitive to random system errors in both the flip angles and evolution terms. Small magnitudes of one half of one percent random error for flip and evolution terms in the model matched the experimental results well.

5. CONCLUSION

The experimental results show reasonably good agreement with theoretical prediction as well as with previous work using an imaging approach for a type II quantum processor. Simulation of the experimental implementation showed excellent agreement with experimental results. Furthermore, the simulation pointed to a high degree of remaining off-axis magnetization terms from the pseudo-pure state preparation as the main contributor of experimental data deviation from the analytical solution. This indicates that an improved implementation the pseudo-pure state, through the improved implementation of high power, low field-distorting gradients, would greatly improved the quality of experimental data.

Further work is in the development an implementation of multiple-coil type II quantum computer system. This system will use the existing custom software already developed along with the custom two full channel spectrometer but will run on a 5 Tesla magnet and employ smaller coils along with a custom constructed hardware switch to control the operation of the

coils. This switch will allow full control of the coils by the software and allow optimization of coil use based on sample fidelity and experimental needs. The additional coils and switch give the advantage of additional computing power with relatively small expensive as compared to adding additional spectrometer channels as well as additional coils. The improved filling factor of the planned smaller coil design, the increased system field strength and the planned modification to the collision operator[26] should result in improved system fidelity and overall system accuracy.

A four coil insert constructed for the multi-coil work is shown in Fig. 11. This insert has a maximum coil off-set of 45 mm from magnet center. This configuration yields acceptable line widths, even off-axis, as shown in Fig. 12.

ACKNOWLEDGMENTS

We would like to acknowledge his indebtedness to the Air Force Office of Scientific Research (AFOSR) and their support of the Quantum Computation for Physical Modeling theme. Long-term support was provided through the Computational Mathematics Program of the AFOSR for algorithm development research beginning in 1992 under the Novel Strategies for Parallel Computing Initiative at the Air Force Research Laboratory.

REFERENCES

1. Jeffrey Yepez, *Int. J. Modern Phys. C* **12**(9), 1273 (2001).
2. Jeffrey Yepez, *Phys. Rev. A* (2006). (To appear).
3. Jeffrey Yepez, *Int. J. Modern Phy. C* **12**(9), 1285 (2001).
4. G. P. Berman, A. A. Ezhov, D. I. Kamenev, and J. Yepez, *Phy. Rev. A* **66**(012310), 8 (2002).
5. Marco A. Pravia, Zhiying Chen, Jeffrey Yepez, and David G. Cory, *Comp. Phys. Commun.* (2001).
6. Jeffrey Yepez, *J Stat. Phys.* **107**(1), 203 (2002).
7. Zhiying Chen, Jeffrey Yepez, and David G. Cory, *Phys. Rev. A* (2005) arXiv:quant-ph/0410198. (submitted).
8. J. H. Noggle and R. E. Schirmer, *The Nuclear Overhauser Effect, Chemical Applications*, (Academic Press, NY, 1971).
9. A. G. Webb, *Prog. Nucl. Magn Reson. Spectrosc*. **31**, 1 (1997).
10. A. Haase, F. Odoj, M. Von Klienlin, I. Warnking, F. Fidler, A. Weisser, M. Nittka, E. Rommel, T. Lanz, B. Kalusche, and M. Griswold, *Concepts Magn. Reson*. **12**(6), 361 (2000).
11. D. I. Hoult and P. C. Lauterbur, *J. Magn. Reson*. **34**(2), 425 (1979).
12. T. L. Peck, R. L. Magin, and P. C. Lauterbur, *J. Magn. Reson. B* **108**, 114 (1995).

13. Jeffrey Yepez, *Quant. Inform. Proc*. DOI: 10.1007/s11128-005-0009-7.
14. Jeffrey Yepez, *Quant. Inform. Proc*. DOI: 10.1007/s11128-005-0008-8.
15. Jeffrey Yepez, *Int. J. Modern Phy. C* **9**(8), 1587 (July 1998).
16. Marco A. Pravia, PhD. thesis, Massachusetts Institute of Technology(2002).
17. Marco A. Pravia, Zhiying Chen, and David G. Cory, arXiv:quant-ph (Mar 2003).
18. Malcolm H. Levitt, *Spin Dynamics: Basics of Nuclear Magnetic Resonance* (Wiley, 2001).
19. F. Bloch, *Phys. Rev.* **70**(7 and 8), 469 (Oct 1946).
20. David G. Cory, Mark D. Price, and Timothy F. Havel. *Phys D* **120**, 82 (1998).
21. Isaac L. Chuang, Lieven M. K. Vandersypen, Xinlan Zhou, Debbie E. Leung, and Seth Lloyd, *Nature* **393**, 143(4) (May 1998).
22. Mark D. Price, Evan M. Forunato, Marco A. Pravia, Craig Breen, Swami Kumaresean, Gabriel Roseberg, and David G. Cory, *Concepts Magn. Reson*. **13**(3), 151 (2001).
23. Marco A. Pravia, Evan Fortunato, Yaahov Weinstein, Mark D. Price, Grum Teklemariam, Richard J. Nelson, Yehuda Sharf, Shyamal Somaroo, C. H. Tseng, Timothy F. Havel, and David G. Cory, *Concepts Magn. Reson*. **11**, 225 (1999).
24. Neil A. Gershenfeld and Isaac L. Chuang, *Science* **275**, 350 (Jan 1997).
25. M. D. Price, S. S. Somaroo, C. H. Tseng, J. C. Gore, A. F. Fahmy, T. F. Havel, and D. G. Cory, *J. Magn. Reson*. **140**(2), 371 (1999).
26. Zhiying Chen, Jeffrey Yepez, and David G. Cory, arXiv:quant-ph, 0410198 (April 2004).